Research Article

Synthesis of Y₃Al₅O₁₂:Eu and Y₃Al₅O₁₂:Eu,Si phosphors by combustion method: Comparative investigations on the structural and spectral properties

Manisha UPASANI[*]

Department of Physics, Rashtrasant Tukadoji Maharaj Nagpur University, Nagpur, India

Abstract: This paper reports the comparative investigations of the structural and spectral properties of $Y_3Al_5O_{12}$:Eu^{3+} (YAG:Eu) and $Y_3Al_5O_{12}$:Eu^{3+},Si^{4+} (YAG:Eu,Si) phosphors synthesized by combustion method at low temperature. A pure phase was identified for the YAG:Eu phosphor with a suitable amount of SiO_2. Rietveld refinement and analytical calculation of different structural parameters were performed to get the idea about the SiO_2 substitution in YAG:Eu. The characteristic red luminescence corresponding to Eu^{3+} transitions was observed after irradiation with ultra violet (UV) light and enhanced with SiO_2 addition. Jorgensen formula and nephelauxetic ratio were used to understand the ligand behavior of Eu–O bond in YAG doped phosphor. The Judd–Ofelt intensity parameters and color properties of the phosphors were determined in detail. An efficient synthesis method for YAG:Eu phosphor, compatible for industrial applications, was proposed.

Keywords: yttrium aluminum garnet ($Y_3Al_5O_{12}$, YAG); light emitting diode (LED); red phosphor; combustion synthesis

1 Introduction

The discovery and growth of novel transparent ceramics for optical applications have introduced demanding research in the field of inorganic optical materials. More recently, a number of studies have shown that polycrystalline ceramics are more beneficial than single crystals. They have advantages of optical transparency and high homogeneity and thermal conductivity. Among other candidates, garnet is a host with excellent structural compatibility. Garnet is mainly synthesized from rare earth and metal oxide and can be described by the $\{A\}_3[B]_2(C)_3O_{12}$ formula, where A is a

dodecahedrally coordinated site with point group D_2 (without an inversion center), while B and C are octahedrally and tetrahedrally coordinated sites with C_{3i} (with an inversion center) and S_4 point groups respectively. Yttrium aluminum garnet ($Y_3Al_5O_{12}$,YAG) is an efficient host matrix. Inner Y^{3+} and Al^{3+} can be substituted by various types of cations with different sizes and valences to a certain extent. It is well known that rare earth ion doped YAG materials have been widely studied in the applications of laser, fluorescence display, and white light emitting diode (LED) [1]. When Y^{3+} ions in YAG doped with trivalent rare earth ions, such as Gd, Eu, Pr, Ce, and Tb, it can be widely used in optoelectronic devices [2–4]. At present, commercial white LED is mainly manufactured by combining a GaN based blue LED chip with $Y_3Al_5O_{12}$:Ce^{3+}

———————————
* Corresponding author.
E-mail: manishaupasani@gmail.com

(YAG:Ce) yellow phosphor [5]. But the LED faces problems of color separation between blue and yellow and poor color rendering caused by the lack of a red component in the spectrum. This drawback can be overcome by using near ultra violet (n-UV) LED chip excited tricolor phosphors or a phosphor supplemented by those emitting at longer wavelength. The use of red and orange-red phosphors is very common for this purpose. However, some of phosphors suffer from luminous intensity degradation, emission color change, and poor heat resistance. For decades, trivalent europium, Eu^{3+}, is an efficient activator for red emitting phosphors due to its characteristic emission resulting from its characteristic transitions of $^5D_{0,1}$–^7F_J ($J = 4, 3, 2, 1, 0$) [6]. Eu activated YAG is also a promising red phosphor that may be widely used in optical display and lighting, and has been reported by many researchers for different purposes [7,8]. Kim *et al*. [9] reported the enhancement of the photoluminescence (PL) by lithium ion incorporation in YAG:Eu^{3+} phosphor. Lu *et al*. [10] reported synthesis and luminescence properties of microemulsion-derived YAG:Eu^{3+} phosphor. In the previous work, Eu^{3+} doped YAG has been synthesized at low temperature [11]. In all mentioned studies, no work has been reported related to the effect of Si on YAG:Eu at low temperature by combustion synthesis for commercial purpose. Generally, high temperature and post heat treatment are required for the synthesis of YAG. It is very difficult to achieve a pure YAG phase at low temperature and without any additional resource of heat treatment. Thus, preparation of YAG as either pure or doped crystalline material is still a hard challenge for materials scientists. In particular, in the present study, attention was focused on the formation of rare earth doped pure YAG phase at low temperature. In the work reported here, Eu doped YAG that exhibited orange-red emission was synthesized and the effect of Si^{4+} codoping on structural and luminescence properties was studied. The Judd–Ofelt intensity parameters and color properties of the phosphors were also determined in detail. Our results revealed that this technological approach enables us to achieve a stable single-phase structure of garnet and orange-red emission of YAG:Eu can be efficiently improved by incorporating a small amount of Si^{4+} ions.

2 Experimental

2. 1 Materials and method

Red emitting phosphor samples YAG:Eu_x ($0.5 \leqslant x \leqslant 2$)

and YAG:Eu,Si (Eu 1 mol% and Si 0.5–5 mol%) were synthesized by controlled one step autocombustion method with mixed fuels. The synthesis process is similar as explained in Refs. [12,13]. Europium and yttrium nitrates were prepared by dissolving their oxides Eu_2O_3 (99.99% pure) and Y_2O_3 (99.9% pure) with nitric acid, respectively. The excess HNO_3 was volatilized by continued and mild heating. The redox reaction was carried out among nitrates and organic fuels. The strict control of the stoichiometry is required to avoid the formation of secondary phases. Stoichiometric amounts of hydrated nitrates of yttrium, aluminium, and europium were carefully mixed with urea/glycine. The nitrate to fuel ratio was calculated by the technique designated as previous [14]. A thick paste formed due to the existence of large amount of water of crystallization in aluminium nitrate. A china dish with the paste was introduced in a preheated furnace at 500 ℃. As the procedure was exothermic, in few minutes the paste foamed, and a flame formed and ended in few seconds. At a certain instance, autocombustion of urea and glycine took place with fire ignited within the dish. The reaction lasted for few minutes and resulted in fluffy voluminous mass. The dish was straight away removed from the furnace, and the fluffy mass was crushed by agate mortar to procure as-synthesized phosphor. YAG:Eu,Si phosphor was also synthesized in the optimized Eu concentration by varying the Si content in the form of silicic acid (SiO_2) as explained above.

2. 2 Characterization

The phase identification of prepared phosphors was carried out by Philips PANalytical X'pertPro diffractometer using monochromatic Cu Kα radiation ($\lambda = 1.5406$ Å) in the 2θ range from 10° to 80°. The scanning electron microscopy (SEM) of the powders was captured with a JEOL electron microscope Model JSM-6380A. Photoluminescence (PL) characteristics were studied using a Hitachi F-4000 spectrofluorimeter using 1.5 nm spectral slit width in the range of 200–700 nm. Fourier transform infrared spectroscopy (FTIR) was measured to characterize the bond stretching vibrational spectrum of the compositions in the phosphors by (ALPHA) FT-IR spectrometer.

3 Results and discussion

3. 1 Structural analysis

All the prepared phosphors were measured and

analyzed by X-ray diffraction (XRD) patterns. The XRD patterns of selected YAG:Eu and YAG:Eu,Si phosphors are revealed in Fig. 1. Comparing the XRD patterns with standard JCPDS cards, the main diffraction peaks of YAG:Eu are all consistent with JCPDS Card No. 33-0040. However, there are some weak diffraction peaks from the impurity phase that can be ascribed to the yttrium aluminum monoclinic (YAM) phase (JCPDS Card No. 34-0368). As SiO_2 is added (1 mol%), the phase-pure YAG is detected. However, with further increase in SiO_2 amount, other impurity phases and even amorphous phase occur (not included in this report). The result indicates that a critical amount value of SiO_2 exists, such as 1 mol% in this experiment, enabling a possibility to obtain pure phase of YAG with small amount of Eu^{3+} ions. This directs that a small amount of Eu^{3+} and Si^{4+} does not change the garnet structure. However, the shift of diffraction angle is detected with addition of Eu^{3+} and Si^{4+} which will be revealed in the following.

The luminescence properties of phosphor particles are dependent on certain characteristics such as crystallite size [15] and crystallinity [16]. Crystallinity is one of the most significant parameters to achieve phosphor particles with maximum luminescence efficiency. The formation of sharp diffraction pattern is the consequence of the generation of high *in situ* temperature during combustion reaction. The sharp peaks in XRD patterns and pure phase formation are the consequences of improved crystallinity. To further investigate the effect of Si addition in the formation of

Fig. 1 XRD patterns of YAG:Eu and YAG:Eu,Si compared with the JCPDS data files.

pure YAG phase and suppression of impurity phases, the structural parameters of as-synthesized phosphors were studied and compared.

3.2 Structural parameters

The structural parameters, such as lattice constant (a), inter-planar spacing (d), crystallite size (D), dislocation density (δ), and microstrain (ε), were calculated from the XRD data. The lattice constant and inter-planar spacing for the main peak at (420) were calculated using the following formulae:

$$\sin^2 \theta = \frac{\lambda^2}{4a^2}(h^2 + k^2 + l^2) \qquad (1)$$

$$d = \frac{a}{\sqrt{h^2 + k^2 + l^2}} \qquad (2)$$

The crystallite size (D) was determined using the Scherrer formula [17] and Williamsons–Hall (W–H) equation [18] as given in the formulae below:

$$D = \frac{0.9\lambda}{\beta \cos \theta} \qquad \text{Scherrer formula}$$

$$\beta \cos \theta = \frac{K\lambda}{D} + \varepsilon \sin \theta \quad \text{Williamsons–Hall equation}$$

where λ is the wavelength of the X-ray radiation, β represents the full width at half maximum (FWHM), θ is the angle of diffraction, and ε represents the microstrain existed in the sample. The peak broadening in prepared phosphors develops not only due to crystallite size but also due to existing strain. In peak broadening, strain and crystallite size effects are not associated with each other and they can be distinguished by W–H plot. W–H analysis is an integral breadth method where size-induced and strain-induced broadenings are known by considering the peak width as a function of 2θ. Strain and crystallite size are calculated from the slope and y-intercept of the fitted line respectively as shown in Fig. 2. The results are in agreement with the Scherrer formula. The basic difference between the two methods is that Scherrer formula follows a $1/\cos\theta$ dependency but not $\tan\theta$ as W–H equation. The microstrain present in the sample was also calculated from the full width at half maximum (FWHM) of the diffraction peaks as given in the formula [19]:

$$\varepsilon = \frac{\beta \cos \theta}{4}$$

The dislocation density δ for the samples can be calculated from the equation:
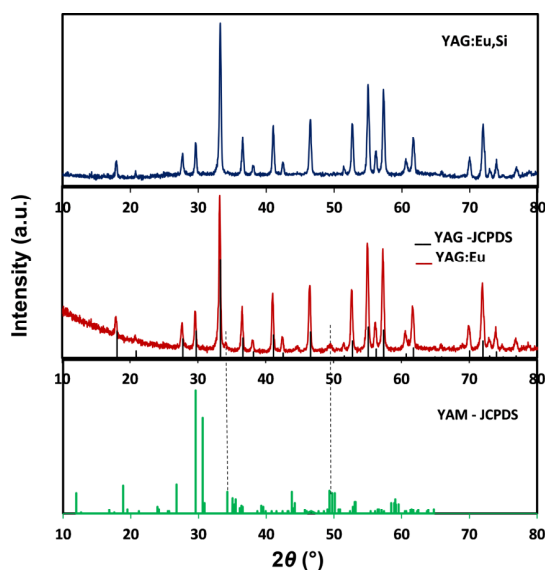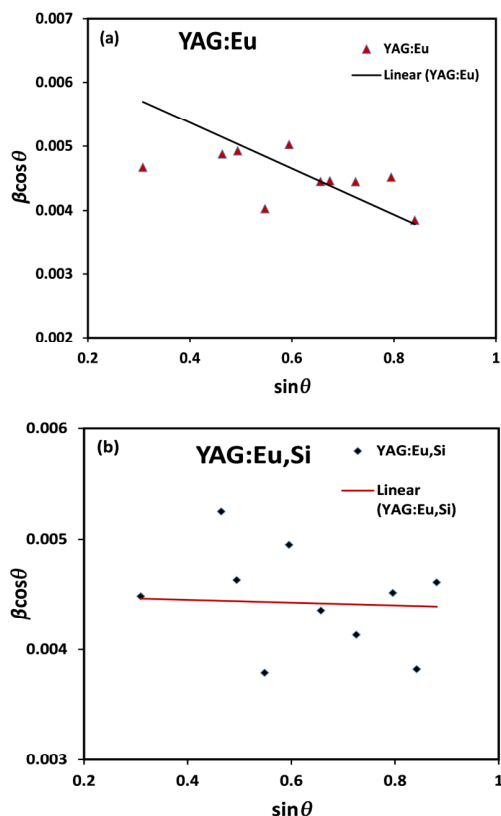
Fig. 2 Williamsons–Hall plots for phosphors.

$$\delta = \frac{1}{D^2}$$

The structural parameters, such as crystallite size, dislocation density, and microstrain, are given in Table 1. The presence of microstrain and dislocation density results from the peak broadening of the XRD patterns.

The estimated crystallite size of YAG:Eu phosphor is found to increase with Si doping. Larger crystallite size decreases the density of the grain boundaries, which might reduce adsorption and/or scattered light generated inside and result in luminescence enhancement. Above results reveal that dislocation density and strain values decrease with Si doping and henceforth result in improvement in crystallinity.

3. 3 Rietveld refinement

A structural refinement by the Rietveld method [20]

Table 1 Structural parameters of YAG:Eu and YAG:Eu,Si phosphors

Phosphor	Crystallite size D (nm)		Dislocation density δ (10^{14} m^{-2})	Microstrain ε	
	Scherrer	W–H		Calculated	W–H (magnitude)
YAG:Eu	10–30	20	25	0.0015	0.0032
YAG:Eu,Si	10–40	31	10	0.0011	0.0001

using MATCH program [21] was performed to analyze the structural and unit cell parameters of the prepared phosphors and shown in Fig. 3. This method uses a least squares method to refine a theoretical profile until it matches the measured profile, and from this refinement, the crystal structure and lattice parameters are attained. By computing the Bragg's contribution (χ^2) and goodness of fit (GOF) parameters, the excellence of structural refinement is checked. This GOF is subject to some reliability factors R_{wp} and R_{exp} as GOF = R_{wp}/R_{exp}.

For perfect refinement, χ^2 must be less than 5 and GOF must approach to unity [20]. For YAG:Eu and YAG:Eu,Si phosphors, the GOF are 0.88 and 0.87, whereas χ^2 are 1.9 and 1.4, respectively. The results designate good agreement among the observed and calculated XRD patterns. Table 2 exhibits ultimate refined structural parameters for as-synthesized phosphors.

A garnet structure can be described as a network of polyhedrons, in which octahedron and tetrahedron are linked by shared oxygen ions at the corners, as represented in Fig. 4. It is well known that in YAG, Y^{3+} ions are at dodecahedral cavities formed by these
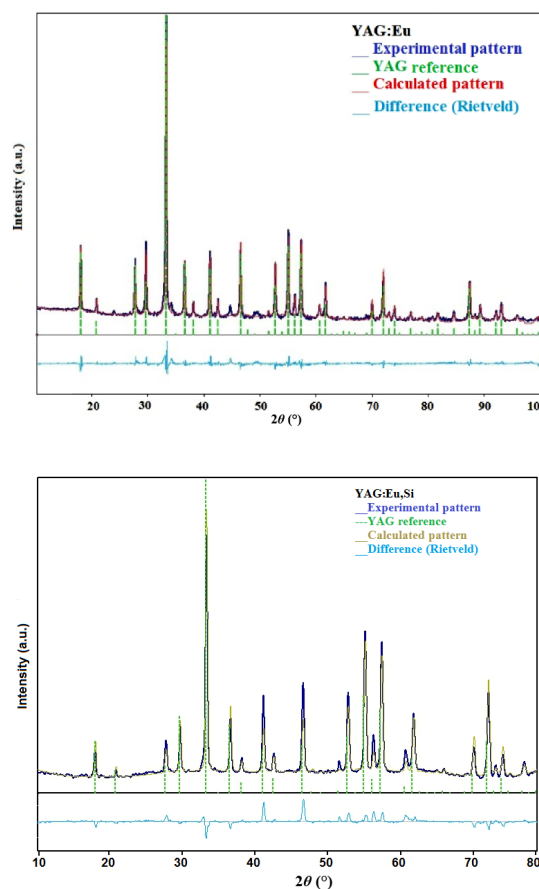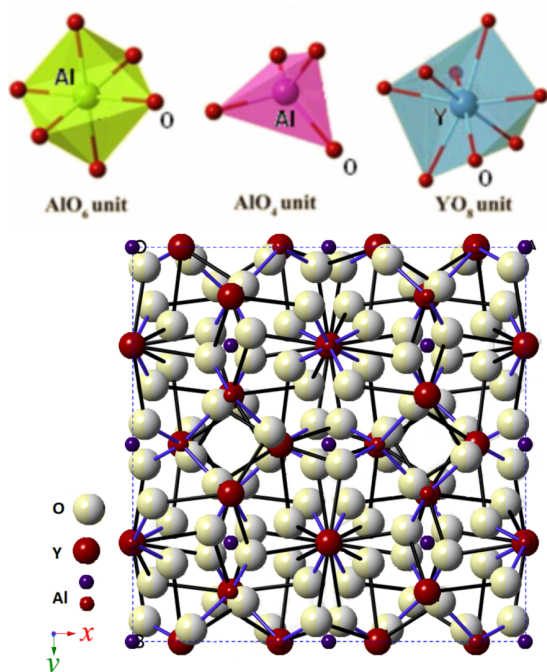

Fig. 3 Rietveld refinement for phosphors.

Table 2 Parameters of phosphors after Rietveld refinement

Phosphor	Atom	Wyckoff	X	Y	Z	Occupancy	Lattice parameter
YAG:Eu	Y	24c	0.125	0	0.25	0.1485	
	Eu	24c	0.125	0	0.25	0.0015	$a=b=c=12.0615$ Å
	Al_1	16a	0.0	0	0.0	0.1000	$d=2.697$ Å
	Al_2	24d	0.375	0	0.25	0.1500	$V=1754.7$ Å^3
	O	96h	−0.02873	0.04985	0.14378	0.6000	
YAG:Eu,Si	Y	24c	0.125	0	0.25	0.1485	
	Eu	24c	0.125	0	0.25	0.0015	
	Al_1	16a	0.0	0	0.0	0.1000	$a=b=c=12.0295$ Å
	Al_2	24d	0.375	0	0.25	0.1475	$d=2.689$ Å
	Si	24d	0.375	0	0.25	0.0250	$V=1740.7$ Å^3
	O	96h	−0.04737	0.02925	0.13638	0.6000	

Fig. 4 Structure of the YAG unit cell.

polyhedral arrangements in chains in three crystallographic directions. Thus YAG:Eu/YAG:Eu,Si garnet has three different cation sites. The Y^{3+} ions are positioned in a 24c dodecahedral D_2 site with a coordination number of 8, and Al^{3+} ions are located in cooperation with 24d tetrahedral S_4 site and 16a octahedral S_6 site with fourfold and sixfold coordinations respectively. The O^{2-} ions reside in 96h site and each is a member of one tetrahedron, one octahedron, and two dodecahedrons [22]. The rare earth ions are expected to mostly enter into the distorted dodecahedral site by exchanging the Y^{3+} ions and to be coordinated to eight O^{2-} ions due to their comparable ionic size.

The relative population of the tetra-coordinated Al^{3+} and hexa-coordinated Al^{3+} sites are 60% and 40% respectively. The ionic radii of the tetra- and hexa-coordinated Si^{4+} ions are 0.26 and 0.4 Å, while those of tetra- and hexa-coordinated Al^{3+} are 0.39 and 0.535 Å, respectively. Accordingly, the substitution of the Al^{3+} ions by the Si^{4+} ions would cause the reduction of the lattice parameters, which indeed is what we observed in the XRD data measured for our samples. Therefore, the replacement of tetrahedral Al^{3+} with Si^{4+} ions results in the reduction of d-spacing in YAG:Eu, in agreement with some other investigations [23,24]. It suggests that introduction of Si^{4+} changes slightly the local crystal field of the matrix. Apart from that, the substitution of Al^{3+} ions with Si^{4+} ions in tetrahedral sites of the crystallographic structure induces Al^{3+} vacancies for preserving the charge neutrality as well as the better substitution of Y (or Eu) with activators in the host. The replacement leads to the occurrence of valence difference. Most likely in such a defect reaction, $4/3Al^{3+} + 1/3V(Al^{3+}) = Si^{4+}$, where $V(Al^{3+})$ signifies the vacancy of Al^{3+}. Thus, to keep the charge balance, the exchange of Si^{4+} for $4/3Al^{3+}$ will produce 1/3 vacancy of Al^{3+}. With the existence of vacancy just by adding suitable amount of SiO_2, there is intensification in diffusion of ions to promote the formation of pure YAG phase at lower temperature.

3.4 Fourier transform infrared spectroscopy

To further investigate the crystallinity and presence of nonradiative groups in the synthesized samples, the FTIR spectra for both YAG:Eu (1 mol%) and YAG:Eu,Si (1 mol%) samples are studied and presented in Fig. 5. It has been reported that emission intensity can be enhanced by reducing nonradiative relaxation rate by removing the atomic groups with high vibration frequencies [24].

The FTIR spectra display bands from 550 to 4000 cm^{-1}. The bands at 786 and 687 cm^{-1} represent the vibrations of Al–O, while the bands at 721 and 568 cm^{-1} are ascribed to Y–O groups [25,26]. From the spectra, it is clear that the separation and sharpness of
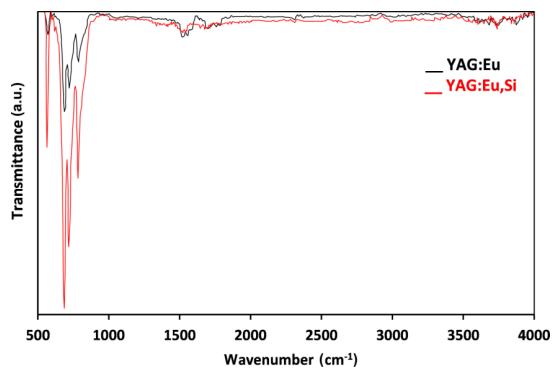
Fig. 5 FTIR spectra of YAG:Eu and YAG:Eu,Si.

Y–O and Al–O peaks increase in YAG:Eu,Si, which specifies intensification in crystallization of YAG. This investigation supports the XRD results. The absorption bands around 1749 and 1557 cm^{-1} originate from C=O and N=O respectively, and are reduced with Si^{4+} doping in YAG:Eu. This directs that the atomic groups with high vibration frequencies reduce with the incorporation of Si and result in enhancement in emission intensity.

3.5 Surface morphology

Figure 6 displays the SEM micrographs of the as-prepared YAG:Eu and YAG:Eu,Si phosphor powders. As shown in Fig. 6, several large pores are revealed on
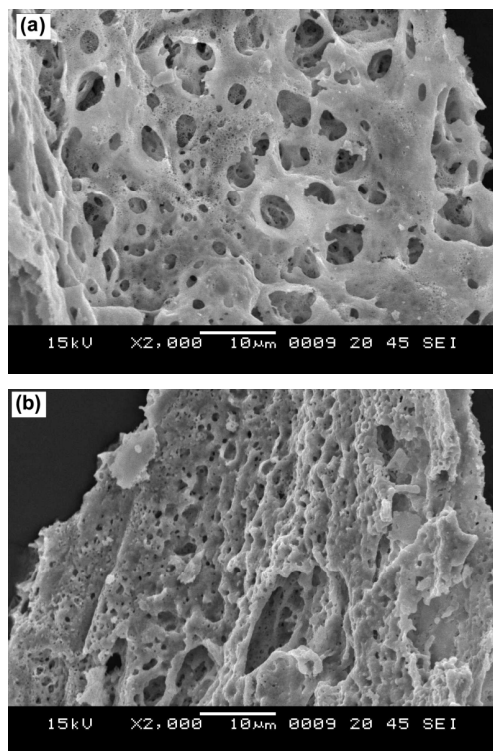

Fig. 6 SEM micrographs of the as-prepared phosphors: (a) YAG:Eu, (b) YAG:Eu,Si.

the surfaces due to evolution of carbon and nitrogen based gases in combustion synthesis. Due to evolution of gases, material forms with porosity which increases after Si doping. Though the reason is not yet clear, increase in porosity may be due to solubility of Si in the matrix.

3.6 Spectral investigation of YAG:Eu and YAG:Eu,Si

Figure 7 illustrates the photoluminescence (PL) excitation spectra. The excitation spectra of YAG:Eu and YAG:Eu,Si phosphors were recorded keeping the emission wavelength at 592 nm. The excitation spectra of these samples are composed of the peaks of f→f electronic transition, which are ascribed to Eu^{3+}–O^{2-} transfer state and the 4f^6 electronic configuration of Eu^{3+} at the range of far ultra violet region. The peak appearing at 395 nm belongs to $^7F_0 \rightarrow {}^5L_6$ electron transition of the Eu^{3+} ions. To achieve half-filled 4f^7 stable configuration, the 4f^6 electronic configuration of Eu^{3+} has to gain one electron.

Thus, when Eu^{3+} is associated to the O^{2-} ligand, there is probability of transfer of one electron from O^{2-} which results in bond formation between Eu^{3+} and O^{2-}. A broad excitation band is detected due to this electron transfer termed as charge transmission band (CTB) located between 200 and 300 nm. This CTB of Eu^{3+} is associated with Eu^{3+}–O^{2-} bond covalency and the symmetry number of Eu^{3+}. The bond covalency of Eu^{3+}–O^{2-} is affected by another metal ion M^{3+} (M^{3+} = Y^{3+}, Al^{3+}) adjacent to O^{2-}. When Al^{3+} site is employed by a smaller Si^{4+} ion, a change in CTB is identified. The peak position of CTB has shifted towards shorter wavelength and the full width at half maxima (FWHM) of the excitation spectrum becomes broader. It was
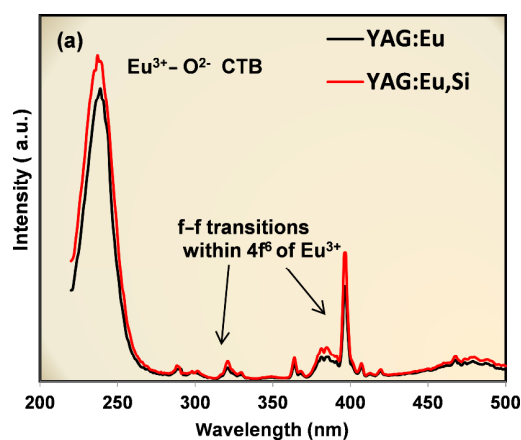

Fig. 7 A comparison of excitation spectra of Y$_{3-x}$Eu$_x$Al$_5$O$_{12}$ ($x = 1$) and Y$_{3-x}$Eu$_x$Al$_{5-y}$Si$_y$O$_{12}$ ($x = y = 1$).

reported that the spectra of the CTB are associated with different factors, i.e., the covalency of the Eu^{3+}–O^{2-} bond, coordination number of Eu^{3+}, and bond length [27]. The reduction in the covalent character of the Eu–O bond results in blue shift of CTB. In general, the band position can be confirmed from Jorgensen formula [28]:

$$\sigma = (\chi_{opt}(X) - \chi_{uncorr}(M))30 \times 10^3 \, cm^{-1} \qquad (3)$$

where σ is the energy of the CTB, $\chi_{opt}(X)$ is the optical electronegativity of the ligand ion which is around the Pauling's electronegativity, and $\chi_{uncorr}(M)$ is the optical electronegativity of the central cation. From the excitation spectra for both samples, the difference in electronegativity values, $\chi(O^{2-}) - \chi(Eu^{3+})$, are 1.394 and 1.406 for YAG:Eu and YAG:Eu,Si phosphors respectively. The increased in the difference in electronegativity value designates the increased in the ionic strength of the Eu^{3+}–O^{2-} bond and hence the covalency decreases. The performance of Eu^{3+}–O^{2-} ligand can also be determined by nephelauxetic ratio (β^-). The nephelauxetic effect is largely attributed to two effects [29]: the reduction of the effective charge on the metal by a covalent bond formation, and the mixing of the metal orbital's with the ligand orbitals. Both effects tend to decrease the electron repulsion in the electronic states of the metals in the complexes. The nephelauxetic parameter (β^-) is regarded as a measure of covalency and expressed mathematically as

$$\beta^- = \frac{1}{n} \frac{\sum \upsilon_{complex}}{\sum \upsilon_{free \, ion}} \qquad (4)$$

where υ is the wavenumber of an absorption transition of Eu^{3+}, and n is the number of detected absorption transitions. The covalency parameter (δ) can be calculated by using the standard relation as [30,31]:

$$\delta = [(1 - \beta^-) / \beta^-] \times 100 \qquad (5)$$

The respective values of β^- and δ for YAG:Eu/ YAG:Eu,Si are 0.99421/0.9967 and 0.5823/0.331. The positive value of nephelauxetic ratio less than one directs the presence of covalent bonding between Eu^{3+} ion and oxygen atom. Thus increase in β^- value with Si^{4+} doping designates the decrease in covalency of the bond which supports our earlier report. The values of the nephelauxetic parameters direct that the possibility of Al–O covalent bonding is higher than that of Si–O bonding. The covalency is checked further by calculating the Judd–Oflet parameters later.

The photoluminescence emission spectra of YAG:Eu phosphor were recorded at excitation wavelengths of $\lambda_{exc} = 239$ and 396 nm. The positions of emission peaks are almost the same for different excitations except the integrated intensity. The maximum emission is observed for 239 nm excitation and presented in Fig. 8.

The emission spectra of both samples show several emission peaks at 592, 611, 652, and 720 nm, corresponding to the respective Eu^{3+} transitions $^5D_0 \rightarrow {}^7F_J(J = 1, 2, 3, 4)$. The large magnitude of the spin–orbit coupling in lanthanides causes the individual J levels of the various electronic terms to be well separated from one another, except for the ground $^7F_0$ and emissive $^5D_0$ states of Eu^{3+}, which are non-degenerated. The various J levels are further split by ligand fields in a maximum of $2J + 1$. By using the transition selection rules for electric dipole (ED) and magnetic dipole (MD) transitions, the number of lines depends on the Eu^{3+} symmetry site, which can be determined by allowed transitions [32]. In accordance with the selection rules $J = 0 \pm 1$ and $\Delta S = 0$, MD transition $(^5D_0 \rightarrow {}^7F_1)$ is allowed, and ED transition $(^5D_0 \rightarrow {}^7F_2)$ is forbidden. But in some cases when Eu^{3+} activators inhabit sites without inversion symmetry, the parity forbiddance is not strictly retained and results in the spectra from the ED transitions [11]. When the Eu^{3+} ion is located at an inversion center, the $^5D_0 \rightarrow {}^7F_2$ emission should be suppressed, and only the $^5D_0 \rightarrow {}^7F_1$ emission should occur [33]. But as in Fig. 8, MD transition is more intense than the ED transition, indicating that the Eu^{3+} ion is located in asymmetrical site without an inversion center. The $^7F_1$ splits in three crystal field sublevels which are belonging to the magnetic dipole nature. Two
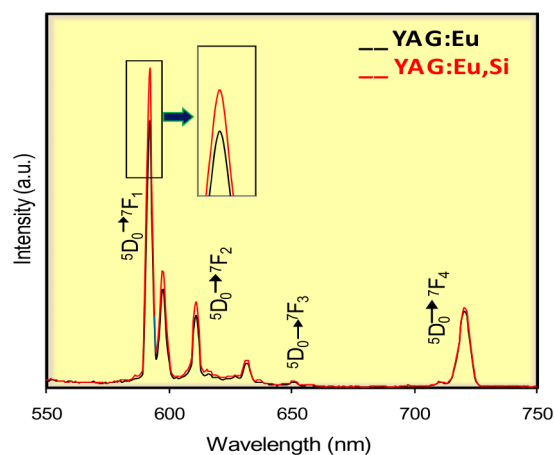
Fig. 8 Comparison of emission spectra of $Y_{3-x}Eu_xAl_5O_{12}$ ($x = 1$) and $Y_{3-x}Eu_xAl_{5-y}Si_yO_{12}$ ($x = y = 1$).

Stark components of this transition are located very close and they are responsible for orange color of YAG:Eu^{3+} emission. The $^5D_0 \rightarrow {}^7F_0$ transition is forbidden, further confirming centrosymmetric nature of the Eu^{3+} site. In D_2 symmetry, $^7F_2$ splits in five sublevels, but only three lines belonging to the electric dipole transition $^5D_0 \rightarrow {}^7F_2$ could be observed and so on.

With increasing Eu^{3+} content until 1 mol% in YAG, the emission intensity increases because of the larger number of luminous centers. A further increase in the Eu^{3+} concentration, however, decreases the intensity as shown in Fig. 9. The intensity decrease might be attributed to the probability of energy transfer among the Eu^{3+} activators due to the shortened distances between them. Thus, the optimal concentration of Eu^{3+} in YAG:Eu determined in this work is 1 mol%.

The decrease in intensity has been attributed to concentration quenching phenomena which involve the nonradiative energy transfer between the same rare earth ions. This transfer of energy may occur via one of the mechanisms: exchange interaction, radiation reabsorption, and multipole–multipole interaction. The concentration quenching will not occur beyond the critical distance. For this reason, it is possible to obtain the critical distance (R_c), which is the shortest distance between the nearest activator ions and can be calculated from the following formula [5]:

$$R_c \approx 2 \left(\frac{3V}{4\pi\chi_c N} \right)^{1/3} \qquad (6)$$

where χ_c is the critical concentration, N is the number of cation sites in the unit cell, and V is the volume of the unit cell. In this case, χ_c of Eu^{3+} in YAG is 1 mol%, $V = 1755$ Å^3, and $N = 8$. Thus, R_c is determined to be

34.73 Å. The value of R_c greater than 5 Å indicates that the multipole–multipole interaction is dominant and is the major cause of concentration quenching. According to Dexter theory [34], the relation between luminescence intensity (I) and activator concentration (x) can be expressed by a modified equation, as follows [35]:

$$\frac{I}{x} = k(1 + \beta(x)^{Q/3})^{-1} \qquad (7)$$

where k and β are constants for the same excitation condition for a given host. According to Eq. (7), the values of Q are 6, 8, and 10 corresponding to dipole–dipole, dipole–quadrupole, and quadrupole–quadrupole interactions respectively, whereas $Q = 3$ corresponds to the exchange interaction. To obtain the correct Q value for the emission, Eq. (7) can be rewritten in logarithmic form as

$$\lg(I/x) = c - (Q/3)\lg x \qquad (8)$$

Since the Q value depends on intensity and concentration of dopants, the dependence of $\lg(I/x)$ and $\lg x$ can be found in Fig. 10.

The graph reports the slope of straight line part as about –1.78, indicating the value of Q equal to 5.34. This value is close to the theoretical value 6 for the electric dipole–dipole (d–d) interaction, implying that the electric d–d interaction is the main cause of the concentration quenching phenomenon.

While keeping Eu^{3+} at the optimal concentration of 1 mol%, the effect of Si^{4+} concentration (from 0.5 to 5 mol%) on excitation and emission was studied and shown for some phosphors in Fig. 7 and Fig. 8. The emission intensity maximizes for 1 mol% Si^{4+} concentration in YAG:Eu (1 mol%). The behavior in emission spectrum of YAG:Eu,Si was compared with that of YAG:Eu in Fig. 8. As the concentration of

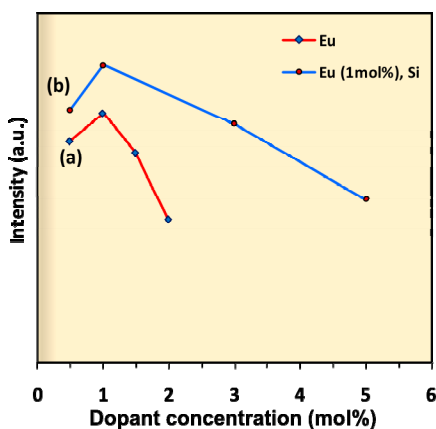**Fig. 9** PL intensity of the MD transition (592 nm): (a) as a function of the Eu^{3+} dopant concentration in YAG; (b) as a function of the Si^{4+} dopant concentration in YAG:Eu.
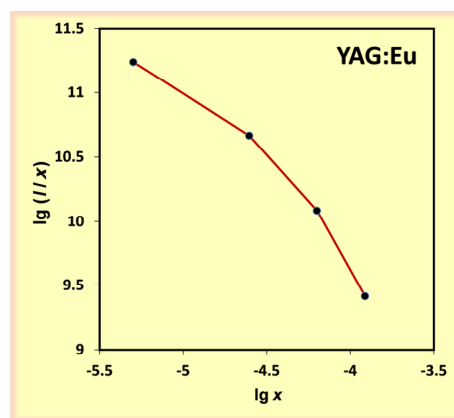

Fig. 10 Logarithmic plot of I/x as a function of the activator concentration x for YAG:Eu.

Si^{4+} increases beyond 1 mol%, emission intensity reduces, as shown in Fig. 9. The enhancement in emission intensity might be related with the modification of the local crystal field around the Eu^{3+} ions due to Si^{4+} doping. The introduction of Si^{4+} ions of smaller ionic size might lower the symmetry around the Eu^{3+} ions. This favors the breaking of forbidden transition of the rare earth ions and promotes the energy transfer from the host to doped rare earth ions. Therefore, the rate of radiation transition enhances. However, this effect becomes prominent only for critical value of Si^{4+} doping. When the Si^{4+} concentration is high, it might develop impurity phases and also cause a large local distortion around lanthanide ions, which can lead to quenching in PL. Apart from this, as explained in previous section, the addition of Si^{4+} ions creates vacancies. These vacancies act as sensitizer for the energy transfer from host to Eu^{3+} ions and result in emission enhancement. From all the above results, it reveals that increased crystallite size, improved crystallinity, densification, and creation of vacancies together are responsible for enhanced photoluminescence.

3. 7 Spectroscopic properties and Judd–Ofelt theory

In this section, spectroscopic properties of synthesized phosphors by Judd–Ofelt theory were studied and compared. The Judd–Ofelt theory has been widely used to calculate the oscillator strengths of the absorption transitions from the ground level to the excited states of rare earth ions in various hosts. Judd–Ofelt (J–O) parameters, $\Omega_t (t = 2, 4, 6)$, can be helpful for understanding the luminescence behavior and site symmetry of rare earth in the matrix [36,37]. The parameter Ω_2 designates for asymmetry behavior and polarization of the rare earth ligands and $\Omega_{4,6}$ depend on the long range effects. However, the Eu^{3+} ions have two special features, which make application of the Judd–Ofelt theory not as straightforward as in the case of other lanthanides. The first one is related to the values of the doubly reduced matrix element of the unit tensor operators between the wave functions of the $4f^6$ configuration. The matrix elements of the $\|U^4\|$ operator are zero for all transitions except for $^7F_1 \rightarrow {}^5D_4$ and $^7F_1 \rightarrow {}^5D_3$ [38,39]. In addition, many transitions observed in the Eu^{3+} absorption spectra have small intensity and the reduced matrix elements are non-zero for a few transitions only like $\|U^2\|^2$ for the $^7F_0 \rightarrow {}^5D_2$

transition and $\|U^6\|^2$ for the $^7F_0 \rightarrow {}^5D_4$ transition. The second feature is that the first excited state of Eu^{3+}, the $^7F_1$ manifold, is only about 300–400 cm^{-1} above the ground state $^7F_0$, which means that even at low temperature, absorption transitions from the $^7F_1$ state contribute to the total absorption spectrum. To overcome these difficulties, the emission spectra of the Eu^{3+} ions are often considered to extract from the Judd–Ofelt intensity parameters. The common procedure is as follows: the intensity of the $^5D_0 \rightarrow {}^7F_1$ magnetic dipole transition is almost host independent, and its radiative transition probability for different hosts is reported to be between 30 and 60 s^{-1} [40,41]. The J–O parameters can be assessed from the luminescence emission spectra by using the technique described by Kodaira *et al*. [39]. The comparative investigation of the radiative behavior of Eu^{3+} in YAG and YAG with Si can be possible by the detail assessment of intensity parameters. The radiative emission rates A_R were calculated in terms of the ratio of areas S under corresponding emission curves as per the equation:

$$\frac{A_R({}^5D_0 \rightarrow {}^7F_{2,4})}{A_R({}^5D_0 \rightarrow {}^7F_1)} = \frac{S({}^5D_0 \rightarrow {}^7F_{2,4})}{S({}^5D_0 \rightarrow {}^7F_1)} \quad (9)$$

where

$$A_R({}^5D_0 \rightarrow {}^7F_2) =$$
$$\frac{64\pi^4 e^2 \vartheta^3}{3h(2J+1)}\left[\frac{n(n^2+2)^2}{9}\right]\Omega_2 \mid \langle {}^5D_0 \parallel U^{(2)} \parallel {}^7F_2 \rangle \mid^2$$

and

$$A_R({}^5D_0 \rightarrow {}^7F_4) =$$
$$\frac{64\pi^4 e^2 \vartheta^3}{3h(2J+1)}\left[\frac{n(n^2+2)^2}{9}\right]\Omega_4 \mid \langle {}^5D_0 \parallel U^{(4)} \parallel {}^7F_4 \rangle \mid^2$$

And all entries have their usual meaning (e is the charge of electron, ϑ is the energy of transition, h is Plank's constant, n is the refractive index, and $J = 0$ for the $^5D_0$ state). For Eu^{3+} emission, the magnetic dipole radiative emission rate $A_R({}^5D_0 \rightarrow {}^7F_1)$ has the value around 50 s^{-1}. The non-zero square reduced matrix elements are $\mid \langle {}^5D_0 \parallel U^{(2)} \parallel {}^7F_2 \rangle \mid^2 = 0.0032$ and $\mid \langle {}^5D_0 \parallel U^{(4)} \parallel {}^7F_4 \rangle \mid^2 = 0.0023$, taken from Ref. [41]. Thus, $\Omega_{2,4}$ values are obtained. Ω_6 could also be estimated by analyzing $^5D_0 \rightarrow {}^7F_6$ transition, but this emission could not be observed due to instrumental limitations. Generally, emission transition can be of several types such as radiative and nonradiative. Radiative transition is the main reason for the light emission. The calculated Judd–Ofelt parameters have been used to predict some important

radiative properties, such as transition probability A_R, radiative lifetime $\tau_{rad}(\psi_J)$, branching ratio $\beta(\psi_J)$, and total radiative transition probability A_T, for the excited states of Eu^{3+} ions. The radiative transition probability for a transition from initial state to final state $\psi_J - \psi'_{J'}$ can be defined as the chance of transition which is radiative and can be calculated from the equation as $A_R(\psi_J, \psi'_{J'}) = A_{J-J'}$.

Since in emission spectra various transitions are present, the totality of all radiative transition probability can be expressed as A_T and can be given as

$$A_T(\psi_J) = \sum_J A_{J-J'} \tag{10}$$

$$\tau_{rad}(\psi_J) = \frac{1}{A_T(\psi_J)} \tag{11}$$

The ratio of each transition to the total radiative transition is known as the branching ratio of that transition and given as

$$\beta(\psi_J) = \frac{A(\psi_J, \psi'_{J'})}{A_T(\psi_J)} \tag{12}$$

In YAG:Eu/Si, Ω_2 intensity parameter describes hypersensitivity of $^5D_0 \rightarrow {}^7F_2$ transition, since it is affected by the symmetry of local surrounding around the Eu^{3+} site. Whereas $\Omega_{4,6}$ are associated with the viscosity and rigidity of the host material which depend on the long range effects. Ref. [42] was used to assess the magnitude of covalency between Eu^{3+} and surrounding ligands. The larger the Ω_2 value, the stronger the covalency. To determine the dominant mechanism, the asymmetry ratio reveals information in the bonding nature between Eu^{3+} ion and the surrounding anions. The asymmetric ratio was calculated by the ratio of the intensity of the electric dipole transition $^5D_0 \rightarrow {}^7F_2$ to magnetic dipole transition $^5D_0 \rightarrow {}^7F_1$. The Judd–Ofelt intensity parameters and the spectral parameters are presented in Table 3.

The decrease in Ω_2 value from YAG:Eu to YAG:Eu,Si indicates the increase in symmetry of Eu^{3+} in the host. This is supported by the asymmetric ratio parameters too. Also the decrease in Ω_2 value indicates

the decrease in covalency which is in agreement with our previous results. The calculated radiative lifetime for $^5D_0$ level for both phosphors is also compared. The decrease in Ω_4 indicates the decrease in rigidity of the host matrix by addition of Si^{4+} ion.

3.9 Color characteristics: CIE parameters

Figure 11 illustrates the color perception related to luminescence of selective YAG:Eu and YAG:Eu,Si samples. Color perception can be stated in terms of the CIE coordinates given by the International Commission for Illumination mathematically. The chromaticity of the phosphor can be determined from x and y parameters (coordinates) on a two dimensional curve, known as chromaticity diagram.

From the chromaticity diagram, it can be seen that the color coordinates traverse towards red region by adding a small amount of Si^{4+} ions in YAG:Eu phosphor. The chromaticity coordinates were calculated for selected phosphor and summarized in Table 4 along with color purity (CP). To check the CP of the emitted color, the formula was adopted as [43]:
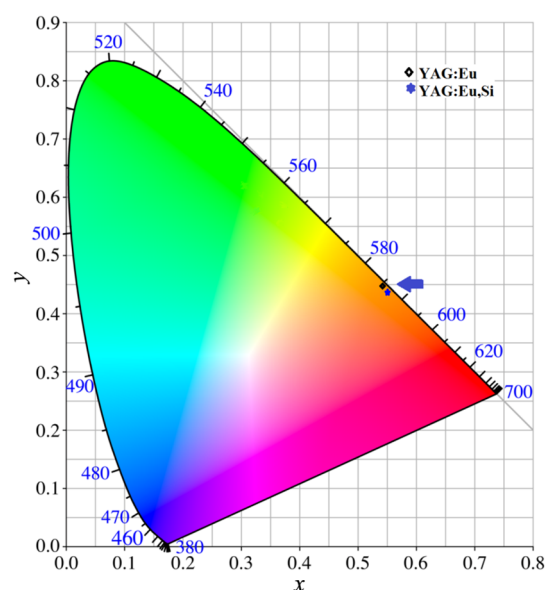

Fig. 11 CIE coordinates for YAG:Eu (1 mol%) and YAG:Eu,Si (1 mol%).

Table 3 Comparative radiative parameters and J–O intensity parameters of YAG:Eu/YAG:Eu,Si phosphors

| Host | J–O intensity parameter | | Transition | $A_{0-2,4}$ (s^{-1}) | A_{0-1} (s^{-1}) | A_T (s^{-1}) | β (%) | τ_{rad} (ms) | Asymmetry ratio |
	Ω_2 (10^{-20} cm^2)	Ω_4 (10^{-20} cm^2)							
YAG:Eu	0.32	1.28	$^5D_0 \rightarrow {}^7F_1$	—	50		49		
			$^5D_0 \rightarrow {}^7F_2$	18.98	—	102.27	18	9.77	0.27
			$^5D_0 \rightarrow {}^7F_4$	33.29	—		33		
YAG:Eu,Si	0.309	1.04	$^5D_0 \rightarrow {}^7F_1$	—	50		52		
			$^5D_0 \rightarrow {}^7F_2$	18.31	—	95.48	19	10.47	0.25
			$^5D_0 \rightarrow {}^7F_4$	27.17	—		29		

Table 4 Color characteristics of YAG:Eu/YAG:Eu,Si phosphors

Phosphor	Color coordinate	Color purity (%)
YAG:Eu	(0.53,0.45)	89.7
YAG:Eu,Si	(0.55,0.44)	91.3

$$\text{Color purity} = \frac{\sqrt{(x_s - x_i)^2 + (y_s - y_i)^2}}{\sqrt{(x_d - x_i)^2 + (y_d - y_i)^2}} \times 100\% \quad (13)$$

where (x_s, y_s) are the coordinates of a sample point, (x_i, y_i) are the coordinates of the Illuminants C (0.3101, 0.3162), and (x_d, y_d) are the coordinates of the dominant wavelength of 592 nm as (0.5864, 0.413) in this study.

The color purity in the case of YAG:Eu,Si phosphor is found to be better than that of YAG:Eu. These results direct that it is possible to synthesize Eu^{3+} doped YAG with better color purity at very low temperature and can be improved by adding a critical concentration of Si^{4+}.

4   Conclusions

In summary, this paper deals with analysis of structural and photoluminescence properties of YAG:Eu and YAG:Eu,Si phosphors synthesized by a novel mixed fuel combustion method. A suitable amount of SiO_2 induces the formation of phase-pure YAG:Eu at low temperature. FTIR and SEM studies confirm the formation of phase-pure YAG:Eu. The addition of SiO_2 improves homogeneity and crystallinity within less reaction time and at low temperature. The optical properties of YAG:Eu and YAG:Eu,Si are characterized by comparing spectral parameters and reveal that YAG:Eu,Si is an efficient phosphor which can be synthesized commercially. The optical parameters determined from this approach are in good agreement with that determined from the conventional method. Suitable CIE, color purity, and enough lifetime make these phosphors as good orange-red emitting component in solid state lighting devices.

References

[1]   Mishra K, Singh SK, Singh AK, *et al*. New perspective in garnet phosphor: Low temperature synthesis, nanostructures, and observation of multimodal luminescence. *Inorg Chem* 2014, **53**: 9561–9569.

[2]   Yang H, Kim Y-S. Energy transfer-based spectral properties of Tb-, Pr-, or Sm-codoped YAG:Ce nanocrystalline phosphors. *J Lumin* 2008, **128**: 1570–1576.

[3]   Potdevin A, Chadeyron G, Boyer D, *et al*. Sol–gel based YAG:Tb^{3+} or Eu^{3+} phosphors for application in lighting sources. *J Phys D: Appl Phys* 2005, **38**: 3251–3260.

[4]   Wang L, Zhang L, Fan Y, *et al*. Synthesis of Nd/Si codoped YAG powders via a solvothermal method. *J Am Ceram Soc* 2006, **89**: 3570–3572.

[5]   Blasse G. Energy transfer in oxidic phosphors. *Phys Lett A* 1968, **28**: 444–445.

[6]   Zhang N, Guo C, Jing H. Photoluminescence and cathode-luminescence of Eu^{3+}-doped $NaLnTiO_4$ (Ln = Gd and Y) phosphors. *RSC Adv* 2013, **3**: 7495–7502.

[7]   Yang HK, Chung JW, Moon BK, *et al*. Photoluminescence investigations of YAG:Eu nanocomposite powder by high-energy ball milling. *Curr Appl Phys* 2009, **9**: e86–e88.

[8]   Uhlich D, Huppertz P, Wiechert DU, *et al*. Preparation and characterization of nanoscale lutetium aluminium garnet (LuAG) powders doped by Eu^{3+}. *Opt Mater* 2007, **29**: 1505–1509.

[9]   Kim JS, Choi BC, Yang HK, *et al*. Low-frequency dielectric dispersion and electrical conductivity of pure and La-doped $SrBi_2Nb_2O_9$ ceramics. *J Korean Phys Soc* 2008, **52**: 415.

[10]   Lu C-H, Huang C-H, Cheng B-M. Synthesis and luminescence properties of microemulsion-derived $Y_3Al_5O_{12}$:Eu^{3+} phosphors. *J Alloys Compd* 2009, **473**: 376–381.

[11]   Upasani M, Butey B, Moharil SV. Photoluminescence study of rare earth doped yttrium aluminum garnet—YAG:RE (RE: Eu^{3+}, Pr^{3+} and Tb^{3+}). *Optik* 2016, **127**: 2004–2006.

[12]   Upasani M, Butey B, Moharil S. Synthesis, characterization and optical properties of $Y_3Al_5O_{12}$:Ce phosphor by mixed fuel combustion synthesis. *J Alloys Compd* 2015, **650**: 858–862.

[13]   Upasani M, Butey B, Moharil SV. Luminescence studies on lanthanide ions (Gd^{3+},Tb^{3+}) doped YAG:Ce phosphors by combustion synthesis. *IOSR-JAP* 2014, **6**: 28–33.

[14]   Kingsley JJ, Manickam N, Patil KC. Combustion synthesis and properties of fine particle fluorescent aluminous oxides. *Bull Mater Sci* 1990, **13**: 179–189.

[15]   Kang YC, Lenngoro IW, Park SB, *et al*. YAG:Ce phosphor particles prepared by ultrasonic spray pyrolysis. *Mater Res Bull* 2000, **35**: 789–798.

[16]   Lee S-K, Yoon H-H, Park S-J, *et al*. Photoluminescence characteristics of $Y_3Al_5O_{12}$:Ce^{3+} phosphors synthesized using the combustion method with various reagents. *Jpn J Appl Phys* 2007, **46**: 7983–7986.

[17]   Scherrer P. Bestimmung der Grösse und der inneren Struktur von Kolloidteilchen mittels Röntgensrahlen (determination of the size and internal structure of colloidal particles using X-rays). *Nachr Ges Wiss Goettingen Math-Phys Kl* 1918: 98–100. (in German)

[18]   Williamson GK, Hall WH. X-ray line broadening from filed aluminium and wolfram. *Acta Metall* 1953, **1**: 22–31.

[19]   Cullity BD. *Elements of X-ray Diffraction*. Reading, Massachusetts, USA: Addison-Wesley Publishing Company, 1956.

[20]   Rietveld HM. A profile refinement method for nuclear and

magnetic structures. *J Appl Cryst* 1969, **2**: 65–71.

[21] Crystal Impact. Match! Available at http://www. crystalimpact.com/match/download.htm.

[22] Galasso FS. *Structure and Properties of Inorganic Solids: International Series of Monographs in Solid State Physics*. New York: Pergamon, 1970: 244.

[23] Nien Y-T, Chen K-M, Chen I-G, *et al*. Photoluminescence enhancement of $Y_3Al_5O_{12}$:Ce nanoparticles using HMDS. *J Am Ceram Soc* 2008, **91**: 3599–3602.

[24] Yang M, Sui Y, Mu H, *et al*. Mechanism of upconversion emission enhancement in $Y_3Al_5O_{12}$:Er^{3+}/Li^+ powders. *J Rare Earth* 2011, **29**: 1022–1025.

[25] Muliuoliene I, Mathur S, Jasaitis D, *et al*. Evidence of the formation of mixed-metal garnets via sol–gel synthesis. *Opt Mater* 2003, **22**: 241–250.

[26] Zhou Y, Lin J, Yu M, *et al*. Synthesis-dependent luminescence properties of $Y_3Al_5O_{12}$:Re^{3+} (Re = Ce, Sm, Tb) phosphors. *Mater Lett* 2002, **56**: 628–636.

[27] Yamase T, Kobayashi T, Sugeta M, *et al*. Europium(III) luminescence and intramolecular energy transfer studies of polyoxometalloeuropates. *J Phys Chem A* 1997, **101**: 5046–5053.

[28] Reisfeld R, Jørgensen CK. *Lasers and Excited States of Rare Earth*. Springer-Verlag Berlin Heidelberg, 1977.

[29] Sathyanarayana DN. *Electronic Absorption Spectroscopy and Related Techniques*. New Delhi, India: Universities Press India Limited, 2001: 109.

[30] Jorgensen C. *Orbitals in Atoms and Molecules*. London: Academic Press, 1962.

[31] Sinha SP. Spectroscopic investigations of some neodymium complexes. *Spectrochim Acta* 1966, **22**: 57–62.

[32] Boyer D, Bertrand-Chadeyron G, Mahiou R. Structural and optical characterizations of YAG:Eu^{3+} elaborated by the sol–gel process. *Opt Mater* 2004, **26**: 101–105.

[33] Forest H, Ban G. Evidence for Eu^{+3} emission from two symmetry sites in Y_2O_3:Eu^{+3}. *J Electrochem Soc* 1969, **116**: 474–478.

[34] Dexter DL. A theory of sensitized luminescence in solids. *J Chem Phys* 1953, **21**: 836–850.

[35] Van Uitert LG, Johnson LF. Energy transfer between rare-earth ions. *J Chem Phys* 1966, **44**: 3514–3527.

[36] Judd BR. Optical absorption intensities of rare-earth ions. *Phys Rev* 1962, **127**: 750–761.

[37] Ofelt GS. Intensities of crystal spectra of rare-earth ions. *J Chem Phys* 1962, **37**: 511–520.

[38] Carnall WT, Fields PR, Rajnak K. Electronic energy levels of the trivalent lanthanide aquo ions. IV. Eu^{3+}. *J Chem Phys* 1968, **49**: 4450–4455.

[39] Kodaira CA, Brito HF, Malta OL, *et al*. Luminescence and energy transfer of the europium (III) tungstate obtained via the Pechini method. *J Lumin* 2003, **101**: 11–21.

[40] Boyer JC, Vetrone F, Capobianco JA, *et al*. Variation of fluorescence lifetimes and Judd–Ofelt parameters between Eu^{3+} doped bulk and nanocrystalline cubic Lu_2O_3. *J Phys Chem B* 2004, **108**: 20137–20143.

[41] Bednakiewicz A, Mech A, Karbowiak M, *et al*. Spectral properties of Eu^{3+} doped $NaGdF_4$ nanocrystals. *J Lumin* 2005, **114**: 247–254.

[42] Babu P, Jayasankar CK. Optical spectroscopy of Eu^{3+} ions in lithium borate and lithium fluoroborate glasses. *Physica B* 2000, **279**: 262–281.

[43] Fang Y-C, Chu S-Y, Kao P-C, *et al*. Energy transfer and thermal quenching behaviors of $CaLa_2(MoO_4)_4$:Sm^{3+},Eu^{3+} red phosphors. *J Electrochem Soc* 2011, **158**: J1–J5.